

Entanglements of an End-Grafted Polymer Brush in a Polymeric Matrix

Robert S. Hoy*

Department of Physics and Astronomy, Johns Hopkins University, Baltimore, Maryland 21218

Gary S. Grest

Sandia National Laboratories, Albuquerque, New Mexico 87185

Received April 23, 2007; Revised Manuscript Received July 20, 2007

ABSTRACT: We analyze the entanglement of polymer brushes embedded in long-chain melts and in good and Θ solvents. Individual entanglements are identified using a modified version of primitive path analysis. Due to entropic collapse, the brushes embedded in the melt are more self-entangled than those in the implicit solvents. The self-entanglement of the brushes in the good and Θ solvents as a function of coverage follows a simple scaling argument. We observe a depletion of entanglements near the systems' confining walls and offer several possible explanations. In the melt-embedded systems, the brushes entangle predominantly with the melt at low coverage and with themselves at high coverage. The peak of the brush–melt entanglement density is highest at an intermediate coverage, but the integrated areal brush–melt entanglement density continues to increase with coverage for the studied systems. This areal density correlates well with earlier measurements of the work of adhesion.

1. Introduction

At high surface coverage, polymer chains grafted at one end to a surface are strongly stretched, forming a polymer brush. Polymers grafted to surfaces have a number of useful applications, including colloidal stabilization and lubrication in small molecule solvents^{1,2} and for increasing adhesion between a surface and elastomers.^{3,4} Theoretical interest in these systems arises from the confinement of the polymeric chains, which leads to configurations that are qualitatively different from those of free chains. Following the early work of Alexander⁵ and de Gennes,⁶ there have been a large number of theoretical and experimental studies of polymeric brushes. For reviews on polymer brushes, see refs 7–10. Both scaling^{5,6} and self-consistent field (SCF)^{7,11–13} calculations predict that in a low molecular weight solvent, above an overlap concentration, the brush height (h) scales with the tethered chain length (N_t) and grafting density (Σ) as $h \sim aN_t\Sigma^x$, where a is the monomer size and x depends on the solvent quality. For a good solvent $x = 1/3$, while in Θ and poor solvents, $x = 1/2$ and 1, respectively. These predictions have been confirmed by computer simulations, using both molecular dynamics (MD)^{8,14} and Monte Carlo (MC)^{15–20} methods, as well as experimentally using the surface force apparatus,^{21–23} small-angle neutron scattering,^{24,25} and neutron reflectivity.^{26–28}

As the molecular weight of the solvent increases, de Gennes⁶ found that mobile solvent chains of the same chemical species as the brush are expelled from the brush as the surface coverage Σ and melt chain length N_m increase. Raphaël et al.²⁹ and Aubouy et al.³⁰ developed this approach further, constructing a phase diagram for (N_m, Σ) . Experimentally, polymeric brushes in a melt have been studied by neutron reflectivity,^{31–34} secondary-ion mass spectrometry,^{35,34} and nuclear-reaction analysis.^{36,37} These experiments agree with the theoretical predictions in that in the presence of mobile chains the brush contracts. The first numerical simulations of a brush immersed

in a polymer melt were carried out by Grest,³⁸ who found that, in agreement with theory, that there was a crossover from a wet to a dry brush as the chain length N_m increased. This crossover has important implications for polymer adhesion, as this phase separation of melt and brush chains reduces entanglements at the interface, since even for melt chains with $N_m \ll N_t$, there is strong segregation of the melt from the brush for high coverage. As a result, adhesion enhancement due to a tethered polymer layer shows a surprising nonmonotonic behavior^{4,39} as a function of Σ . Initially the work of adhesion increases as the coverage increases. However, as Σ continues to increase, the tethered chains begin to overlap and phase separate from the melt. In this regime, the interpenetration of the tethered chains into the polymer melt decreases with increasing Σ and as a result the work of adhesion decreases. At sufficiently high coverage, the polymer melt is completely expelled from the tethered chains, thereby causing the work of adhesion to fall off to the bare value due to dispersion forces only.⁴

Recently, it has been shown that Edward's original concept of a primitive path⁴⁰ can be applied to computer-generated polymer melts to identify polymer entanglements. Everaers and collaborators performed "primitive path analysis" (PPA)^{41,42} and obtained results for the entanglement length N_e in agreement with the predictions of a chain-packing model⁴³ that explains trends in rheological simulations^{41,44} and experimental results^{43,45–48} for melts and semidilute solutions of linear homopolymers. The PPA technique, suitably modified, can be used to obtain information about the behavior of *individual* entanglements, which has not been accessible through other theoretical^{49,50} or experimental means.

Here we apply the PPA to identify the entanglements for a polymer brush in contact with a polymeric matrix. All simulations are for a coarse-grained model⁵¹ in which monomers are represented by beads connected by springs. This allows us to study highly entangled polymer systems. All of the results presented here are for long grafted chains of length $N_t = 501$

* Corresponding author. E-mail: robhoy@pha.jhu.edu.

beads, where the entanglement length in a melt is approximately $N_e \sim 70$.⁵² The polymeric matrix studied consists of melt chains of length $N_m = 1000$ beads.

We begin by measuring the brush–brush entanglement density $[\rho_e^{bb}(z)]$ for melt-embedded systems as well as for the same brushes in implicit good and Θ solvents. $\rho_e^{bb}(z)$ increases rapidly with Σ for all systems studied. The extent of the brush increases with increasing solvent quality, while $\rho_e^{bb}(z)$ decreases due to the lower brush density. The melt is a very poor solvent for the brushes, which collapse near the wall to which they are grafted.⁶ Due to this collapse, the integrated, areal entanglement density $[\Omega_e^{bb}(\Sigma)]$ is much higher for the melt-embedded systems than for the implicit solvent systems. The calculated $\Omega_e^{bb}(\Sigma)$ for the good and Θ solvent systems are well fit by a simple scaling argument: $\Omega_e^{bb}(\Sigma) \propto \Sigma^{2-x}$.

Next we examine the brush–melt entanglement density $[\rho_e^{bm}(z)]$ for the melt-embedded brushes. $\rho_e^{bm}(z)$ increases rapidly with Σ , but even at low Σ there is considerable brush–melt entanglement. There is a clear crossover from dominance of brush–melt entanglements to brush–brush entanglements as coverage increases. We also examine the integrated areal brush–melt entanglement density $[\Omega_e^{bm}(\Sigma)]$. This increases monotonically with Σ for the systems studied. As expected, $\Omega_e^{bm}(\Sigma)$ correlates well with measurements of the work of adhesion W^* performed by Sides et al.⁵³ for the same brush–melt systems. However, the correlation is nonlinear; Ω_e^{bm} is sublinear in Σ while W^* is supralinear. This may be attributable to changes in the adhesive failure mechanism with increasing Σ .

In the next section, the simulation method is described. In section III, we present the results of our entanglement analyses. Finally, in section IV we conclude.

2. Polymer Model and Entanglement Analysis Method

We employ a coarse-grained bead–spring polymer model⁵¹ that incorporates key physical features of linear homopolymers, such as covalent backbone bonds, excluded-volume and adhesive interactions, and the topological restriction that chains cannot cross. All monomers have mass (m) and interact via the truncated and shifted Lennard-Jones potential

$$U_{LJ}(r) = 4\epsilon \left[\left(\frac{\sigma}{r} \right)^{12} - \left(\frac{\sigma}{r_c} \right)^{12} - \left(\frac{\sigma}{r} \right)^6 - \left(\frac{\sigma}{r_c} \right)^6 \right] \quad (1)$$

where r_c is the potential cutoff radius and $U_{LJ}(r) = 0$ for $r \geq r_c$. We express all quantities in terms of the length (σ), energy (ϵ), and time ($\tau_{LJ} = \sqrt{m\sigma^2/\epsilon}$).

Covalent bonds between adjacent monomers on a chain are modeled using the finitely extensible nonlinear elastic (FENE) potential⁵¹

$$U_{FENE}(r) = -\frac{1}{2}kR_0^2 \ln(1 - (r/R_0)^2) \quad (2)$$

where $k = 30k_B T/\sigma^2$, T is temperature, and $R_0 = 1.5\sigma$. All simulations of the brush–melt systems and good-solvent brushes are run at $T = 1.0\epsilon/k_B$ and $r_c = 2^{1/6}\sigma$, while the Θ -solvent brushes are run⁵⁴ at $T = T_\Theta = 3.18\epsilon/k_B$ and $r_c = 2.5\sigma$. We also simulated brushes in an implicit poor solvent with $T = 1.5\epsilon/k_B$ and $r_c = 2.5\sigma$ at coverages $\Sigma\sigma^2 = 0.008$ and 0.03 . The good-solvent brushes have equilibrium bond length $l_{gs} = 0.96\sigma$ while the Θ -solvent brushes have equilibrium bond length $l_\Theta = 0.91\sigma$.

For the brush–melt systems, n_t tethered chains and n_m melt chains are placed in a simulation cell of size $L_x \times L_y \times L_z$ with $L_x = L_y$ and $L_z = 154\sigma$. The monomer density $\rho = 0.85/\sigma^3$. All melt chains have $N_m = 1000$ monomers. All brush chains have $N_t = 501$ monomers and are tethered at one end to randomly located

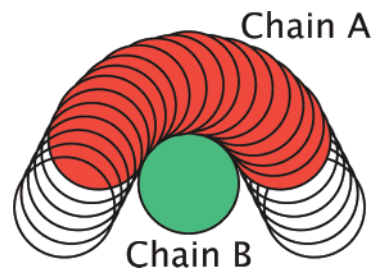


Figure 1. Two-dimensional schematic of entanglement identification. For simplicity of visualization, we depict chain B as lying perpendicular to the page.

Table 1. Surface Coverage (Σ), Number of Tethered Chains (n_t), and Number of Melt Chains (n_m) and Length (L_x) for the Brush–Melt Systems Studied

$\Sigma\sigma^2$	n_t	n_m	L_x/σ	$\Sigma\sigma^2$	n_t	n_m	L_x/σ
0.008	30	476	61.2	0.03	50	193	40.8
0.01	50	630	70.7	0.05	50	106	31.6
0.02	50	302	50.0	0.07	100	137	37.8

points on the $z = 0$ plane with density Σ . The wall at $z = L_z$ is bare. The implicit solvent systems all have $n_t = 500$ chains with $N_t = 501$. Periodic boundary conditions are applied in the x and y directions. Parameters for the brush–melt systems are given in Table 1. These systems are a subset (excluding the highest coverages) of those studied in ref 53.

Equilibration of brush–melt systems with long chains is non-trivial because of the slow diffusive dynamics; the systems in this study were thoroughly equilibrated using a double-bridging hybrid method described extensively in ref 53. In addition to standard MD equilibration, Monte Carlo moves that alter the connectivity of chain subsections were periodically performed, allowing the chain configurations to relax more rapidly.^{55,56} Brushes in implicit solvents are more easily equilibrated. These systems were created by tethering straight chains randomly to the plane at $z = 0$, with the restriction that no two tether points are within 2σ of each other. Newton's equations of motion were then integrated for $10^7\delta t$ with the velocity–Verlet method,⁵⁷ where the time step $\delta t = 0.01\tau_{LJ}$ for the good-solvent case and $\delta t = 0.005\tau_{LJ}$ for the Θ -solvent case. During equilibration, all systems studied were coupled to a heat bath using a Langevin thermostat^{58,51} with damping time $2\tau_{LJ}$. The interactions with the planar substrate were modeled using an integrated LJ potential

$$U_{LJ}^{\text{wall}}(z) = \frac{2\pi\epsilon_{\text{wall}}}{3} \left[\frac{2}{15} \left(\frac{\sigma}{r} \right)^9 - \left(\frac{\sigma}{r} \right)^3 \right] \quad (3)$$

for $z < 2.2\sigma$ and $U_{LJ}^{\text{wall}} = 0$ for $z > 2.2\sigma$, with $\epsilon_{\text{wall}} = 0.1\epsilon$. Since $k_B T \gg \epsilon_{\text{wall}}$, the walls are effectively repulsive.

After equilibration is completed, we perform primitive path analyses as in refs 41 and 59. All chain ends are fixed in space and several changes are made to the interaction potential. U_{LJ}^{wall} is cut off at its minimum at $z = (2/5)^{1/6}\sigma$. Intrachain excluded-volume interactions are deactivated, while interchain excluded-volume interactions are retained. The covalent bonds are strengthened by setting $k = 100\epsilon/\sigma^2$, and the bond lengths are capped at 1.2σ to prevent chains from crossing one another.⁴² We do not attempt to preserve self-entanglements, but their number in melts of the same density is negligible.⁴² The system is then coupled to a heat bath at $T = 0.001\epsilon/k_B$ so that thermal fluctuations are negligible, and the equations of motion are integrated until the chains minimize their length. This typically requires $\sim 1000\tau_{LJ}$. The FENE potential is linearized for $r < R_0/2$ so that the length minimization takes place at constant tension.⁵⁹ Results for brushes embedded in the melt are an average of over 10–20 statistically independent systems, while those for brushes in good and Θ solvents are averaged over two to six configurations.

While standard PPA gives the correct number of entanglements, the procedure is not sufficient to identify individual entanglements.

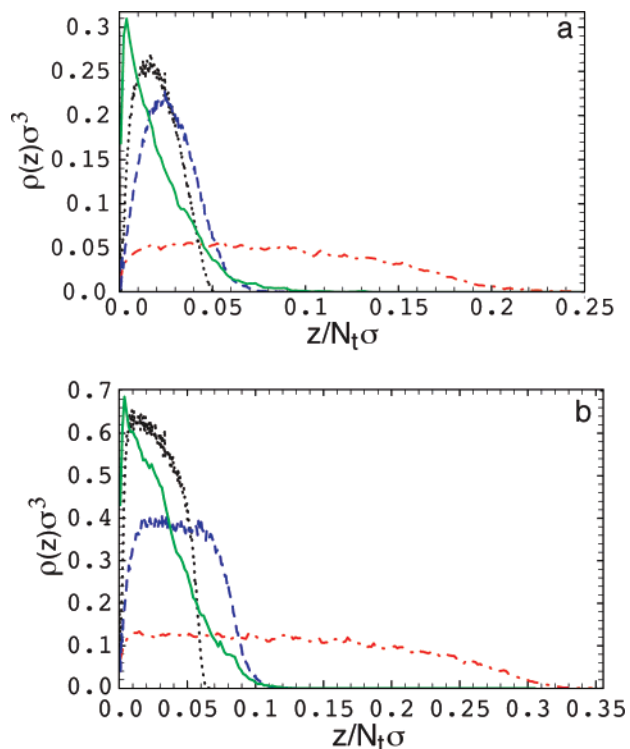


Figure 2. Brush monomer density $\rho(z)$ for a brush embedded in a melt (solid), poor solvent (dotted), Θ solvent (dashed), and good solvent (dash-dotted) at coverages (a) $\Sigma\sigma^2 = 0.008$ and (b) $\Sigma\sigma^2 = 0.03$.

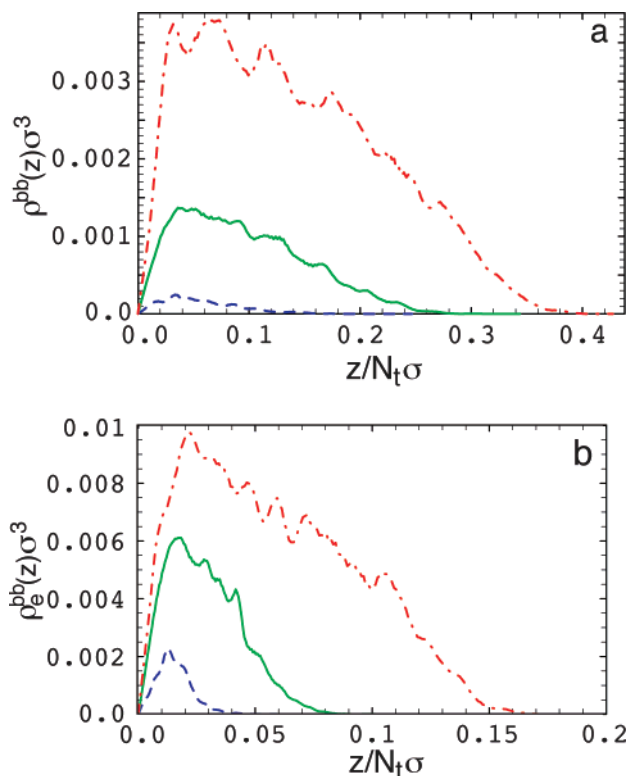


Figure 3. Brush-brush entanglement density ρ_e for $\Sigma\sigma^2 = 0.008$ (dashed), $\Sigma\sigma^2 = 0.03$ (solid), and $\Sigma\sigma^2 = 0.07$ (dash-dotted) for (a) good solvent and (b) Θ solvent.

In the standard PPA method,⁴² the chains maintain the same diameter during the length minimization process. As a result, a high percentage of monomers have interchain contacts, many of which may not represent true entanglements. In addition, the excluded volume may allow the formation of trapped unentangled loops.⁶⁰ For this reason, we extend the analysis of Everaers et al.⁴¹ by

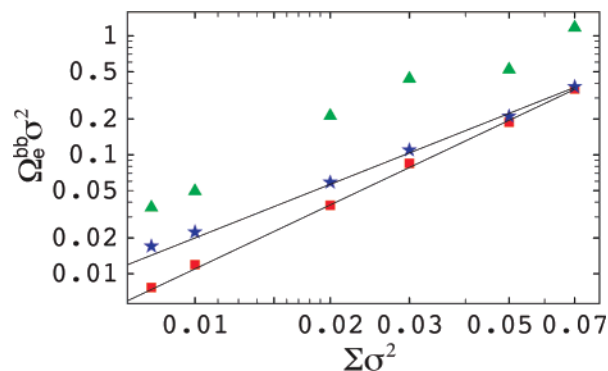


Figure 4. (a) Brush-brush Ω_e^{bb} for melt-embedded brushes (triangles) and brushes in implicit good (squares) and Θ (stars) solvents. The fits to $\Omega_e^{bb}(\Sigma)$ for the good- and Θ -solvent brushes are $\Omega_e^{bb} \propto \Sigma^{1.78}$ and $\Omega_e^{bb} \propto \Sigma^{1.50}$, respectively.

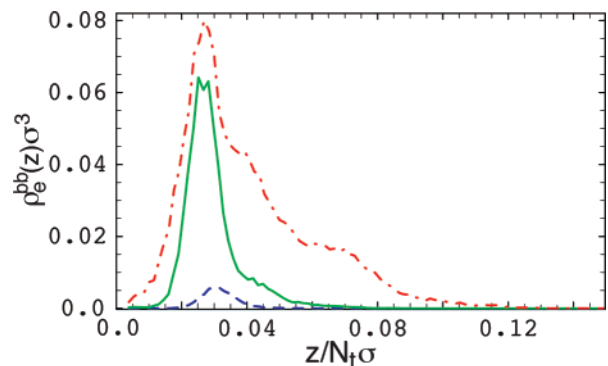


Figure 5. Brush-brush entanglement density $\rho_e^{bb}(z)$ for $\Sigma\sigma^2 = 0.008$ (dashed), $\Sigma\sigma^2 = 0.03$ (solid), and $\Sigma\sigma^2 = 0.07$ (dash-dotted) for melt-embedded brushes.

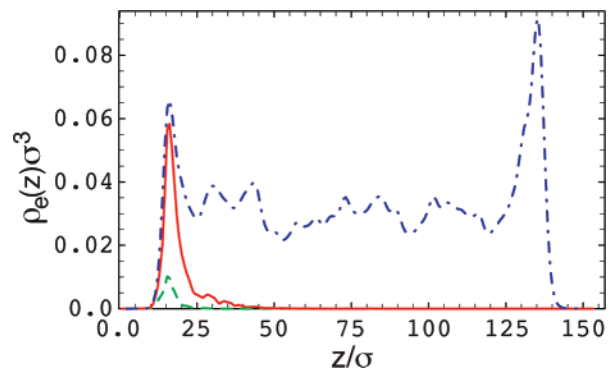


Figure 6. Brush-brush (dashed), brush-melt (solid), and melt-melt (dash-dotted) entanglement densities for $\Sigma\sigma^2 = 0.01$.

introducing extra beads to reach the limit of zero thickness chains in a manner analogous to the work of Tzoumanekas and Theodorou.⁶⁰

At the end of the standard PPA, $n_{dec} - 1$ new beads are placed between adjacent beads on the original chains. (Insertion of extra beads at fixed bead diameter was performed previously and does not affect PPA results: S. K. Sukumaran, private communication.) The bead diameter (i.e., range of the LJ potential), range of U_{LJ}^{wall} , and R_0 are reduced to $1/n_{dec}$ of their initial values. The bonds are further strengthened by setting $k = 100n_{dec}/\sigma^2$, and their lengths are capped at $1.2\sigma/n_{dec}$ to avoid chain crossings. The equations of motion are integrated until the chains again minimize their length after another $\sim 1000\tau_{LJ}$. We found $n_{dec} = 8$ to be sufficiently high to get converged results for entanglement density profiles and use this value in the remainder of the paper. The rapid quench and use of thin chains suggest that our results are similar to those which would be obtained by the other PPA-like methods.^{61,62}

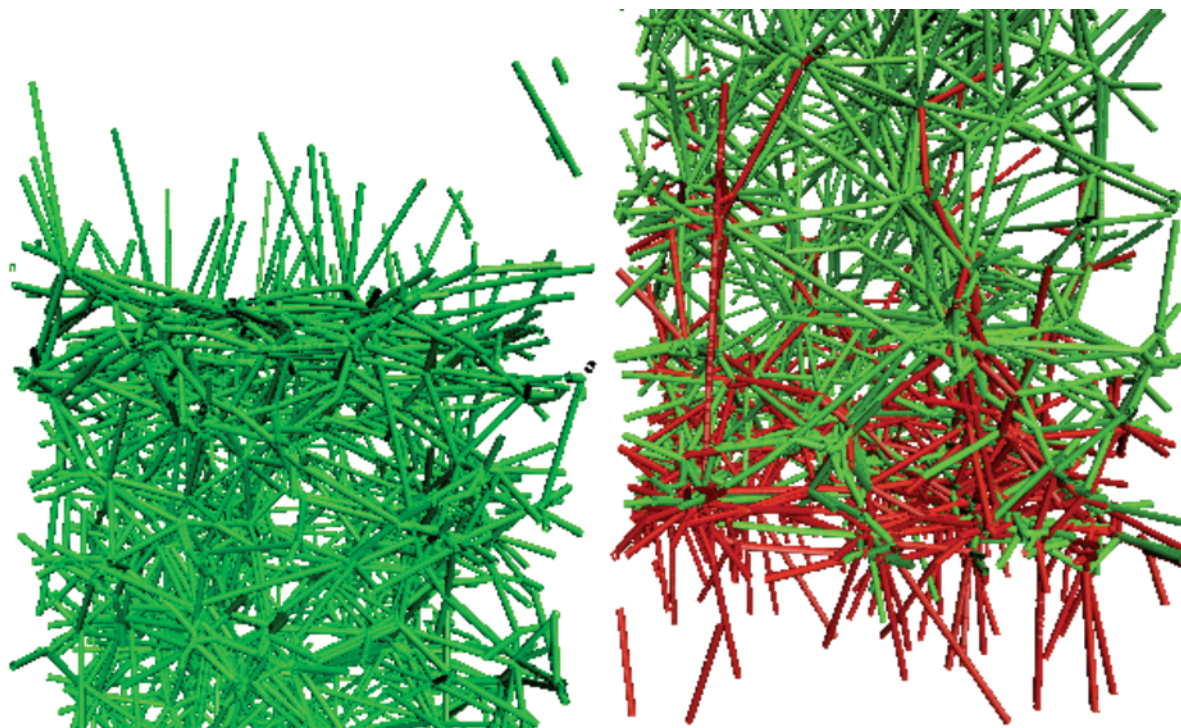


Figure 7. (Color online) a) top, b) bottom of thin-chain PPA end state for one configuration at coverage $\Sigma\sigma^2 = 0.03$. Brush chains are red and melt chains are green. The cross sections depicted are approximately 40σ across and 50σ high.

The average primitive path length (L_{pp}) is a convenient measure of the entanglement length in a homogeneous system,⁶² but since we are interested in identifying individual entanglements, we use an alternate procedure. One entanglement between chains A and B is a block of consecutive monomers on chain A having interchain contacts with chain B, as shown in Figure 1. One entanglement typically involves many monomers, because the reduced bond length is small compared to the bead diameter; the angle between the two sections of chain A attached to the entanglement is often large, so chain A “wraps around” chain B. Identifying the number of entanglements through interchain “contacts” requires care. Setting the contact radius r_{con} equal to the interaction cutoff r_c overestimates the number of entanglements, because when defined this way some monomers in the middle of one true entanglement are often out of contact with the other chain. Setting the contact radius too high also overestimates the number of entanglements. We set r_{con} to the value at which the counted number of entanglements is minimized, approximately $5r_c/4$, i.e., $r_{con} = (5/4)(1/8)2^{1/6}$.

For computational simplicity, we assume all entanglements are binary, i.e., involve only two chains. This may lead to an overestimate of the number of entanglements, because a ternary entanglement (a vertex including three chains A, B, C) is counted as three entanglements: A–B, A–C, and B–C. Because of these approximations, the absolute values of the entanglement densities given should be considered uncertain to an order of 10%. However, the relative values of brush–brush vs brush–melt entanglement densities should be represented very accurately.

3. Results

3.1. Brush–Brush Entanglements. Figure 2 shows the brush monomer density $[\rho(z)]$ for the good, Θ , and poor solvent systems and the brush–melt systems at coverages $\Sigma\sigma^2 = 0.008$ and $\Sigma\sigma^2 = 0.03$. Reference 53 shows $\rho(z)$ for the brush–melt systems for the other coverages considered here. The brush density in the melt-embedded systems is sharply peaked near the wall and has a much lower average height than even the poor solvent system. The melt is clearly a very poor solvent for the brush, as the brush collapses near the wall. As the solvent quality increases, so does the extent of the brush. The maximum

density and extent of the brush in all four cases increases with increasing Σ , as expected.

Figure 3 shows representative brush–brush entanglement densities for the good- and Θ -solvent brushes over the full range of coverages. The “noise” in $\rho_e^{bb}(z)$ is due to the finite number of the systems. Entanglements tend to locally cluster rather than be uniformly distributed. The fluctuations in $\rho_e^{bb}(z)$ reflect fluctuations in the (squared) monomer density at the end of the PPA. As expected from Figure 2, the good-solvent brushes have lower peaks in $\rho_e^{bb}(z)$, but the entanglements extend to larger z . The Θ -solvent brushes are 2–5 times more entangled than the good solvent brushes at the peaks of $\rho_e^{bb}(z)$, but the peaks are narrower. The extent of $\rho_e^{bb}(z)$ (range of z over which $\rho_e^{bb}(z) > 0$) increases rapidly with increasing Σ , as expected. Figure 4 shows the total, integrated number of brush–brush entanglements per unit area $\Omega_e^{bb}(\Sigma)$, where

$$\Omega_e^{bb} = \int_0^{z_{max}} \rho_e^{bb}(z') dz' \quad (4)$$

The Σ -dependence of Ω_e^{bb} for the good- and Θ -solvent brushes can be understood through a simple scaling argument. Assuming a step-function density profile⁵ and uniform brush height h , Ω_e^{bb} should be proportional to $\phi^2 h$, where $\phi \equiv \Sigma/h$ is the concentration of the brushes. Then $\Omega_e^{bb} \propto \Sigma^2/h$ gives $\Omega_e^{bb} \propto \Sigma^{2-x}$. For a good solvent this scaling predicts an exponent of $2 - x = 5/3$ while for the θ solvent $2 - x = 3/2$. A least-squares fit to the data gives exponents of 1.78 ± 0.14 for the good solvent and 1.50 ± 0.16 for the Θ solvent, in very good agreement with the scaling prediction.

Figure 4 also shows Ω_e^{bb} for melt-embedded brushes. The brush–brush entanglement densities in these systems are clearly much higher than those for the brushes in good or Θ solvents. This is expected from the monomer density profiles $\rho(z)$ as the strong exclusion of the melt from the brush significantly increases the number of brush–brush entanglements. Figure 5

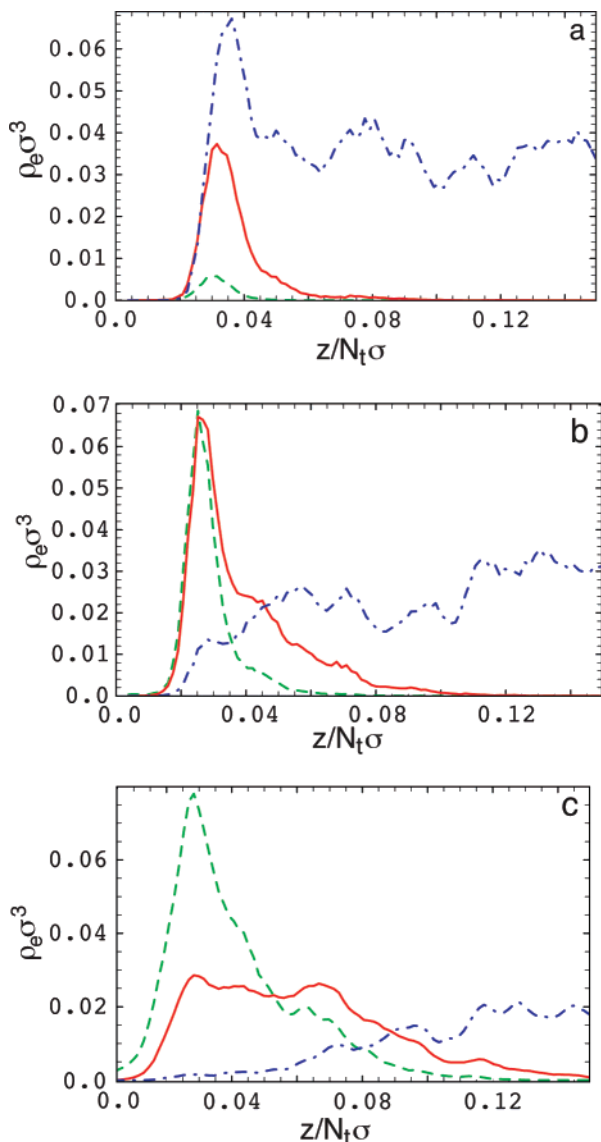


Figure 8. Brush–brush (dashed), brush–melt (solid) and melt–melt (dash-dotted) entanglement densities $\rho_e^{bb}(z)$, $\rho_e^{bm}(z)$, and $\rho_e^{mm}(z)$ for (a) $\Sigma\sigma^2 = 0.008$, (b) $\Sigma\sigma^2 = 0.03$, and (c) $\Sigma\sigma^2 = 0.07$.

shows $\rho_e^{bb}(z)$ for melt-embedded brushes for the same three coverages shown in Figure 3. Note that the peak in the brush–brush entanglement density is displaced from the wall even though the peak in the monomer density $\rho(z)$ is at the wall. We return to this point in the next section.

3.2. Brush–Melt Entanglement. Figure 6 shows brush–brush, brush–melt, and melt–melt entanglement densities for $\Sigma\sigma^2 = 0.01$. The most prominent features are reduced $\rho_e(z)$ at both walls for all three types of entanglements and a large peak in the melt–melt $\rho_e^{mm}(z)$ near the bare wall (large z). The reduction in $\rho_e^{mm}(z)$ near the bare wall agrees with recent PPA observations^{63,64} and experimental evidence for reduced entanglement densities in thin films.⁶⁵ One possible reason for the apparent decrease in entanglement density near the walls is that the entanglements may be biased toward self-entanglements rather than mutual entanglements.⁶⁶ Standard PPA does not capture self-entanglements, and there may be an excess in self-entanglement density near the wall due to the reduced chain dimensions along z .^{67,68} Another possible reason is that there are no chains to entangle with outside the walls, and the chain tension present in PPA pulls entanglements further inside the system. This would explain the peak in $\rho_e^{mm}(z)$ at high z and

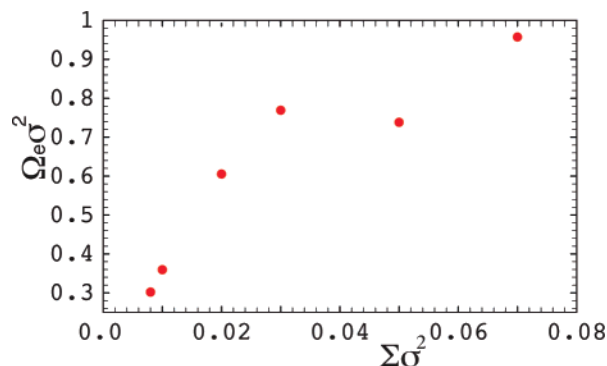


Figure 9. $\Omega_e^{bm}(\Sigma)$ for all the coverages considered in this paper. Results for each Σ are an average over ten statistically independent systems.

the peak at low z coinciding with the peak of the brush–melt $\rho_e^{bm}(z)$. The latter peak is greatest for $\Sigma\sigma^2 = 0.008$ and disappears for $\Sigma\sigma^2 \geq 0.02$, as shown in Figure 8.

Figure 7 shows the top and bottom sections, corresponding to $z > 104\sigma$ and $z < 50\sigma$, respectively, of the thin-chain PPA end state for one configuration with $\Sigma\sigma^2 = 0.03$. Long straight segments terminate in sharp junctions (entanglements) for both brush and melt chains. The ends of the chains near the top and bottom walls are clearly unentangled, consistent with Figure 5. The high- z peak in $\rho_e^{mm}(z)$ evidently corresponds to a region of high melt monomer density at the end of the PPA. Indeed, we find that for entanglements between chains of type A and B, where A and B can each be brush or melt, that the entanglement density $\rho_e^{AB}(z)$ is proportional to the product of the relevant monomer densities, $\rho_A(z)\rho_B(z)$, at the end of the PPA.

Figure 8 depicts brush–brush, brush–melt, and melt–melt entanglement densities for the three coverages $\Sigma\sigma^2 = 0.008$, 0.03, and 0.07. The peak of $\rho_e^{bm}(z)$ is always at $z \approx 15\sigma$, but the width of the peak increases dramatically with increasing Σ . For $\Sigma\sigma^2 = 0.008$, there is negligible brush–melt entanglement above $z = 30\sigma$, while for $\Sigma\sigma^2 = 0.07$, there is significant entanglement up to $z = 50\sigma$. This reflects the increasing height of the brushes.

At low z , the crossover between a preponderance of brush–melt entanglements and a preponderance of brush–brush entanglements clearly occurs at $\Sigma\sigma^2 \approx 0.03$. At this coverage the peaks of the brush–brush and brush–melt entanglement densities are of nearly equal height. For higher coverages the peak of the brush–brush entanglement density is higher, the reverse of the situation for lower coverages. The results are in general consistent with increasing phase separation as Σ increases.

Sides et al. examined⁵³ the work of adhesion (W^*) for the systems considered in this paper (cooled to the glassy state), as well as similar systems at higher Σ . At low pull velocities, W^* increased monotonically with Σ for the range of Σ studied here. One would like to relate W^* to the number of brush–melt entanglements, as shown in Figure 9. W^* correlates very well with the total number of entanglements per unit area Ω_e^{bm} , which within our error increases monotonically with Σ . The correlation, however, is highly nonlinear. Ω_e^{bm} is sublinear in Σ due to the abovementioned phase separation. W^* is supralinear in Σ , showing that, at the coverages considered here, the strengthening effect of the gradual transition from chain scission to crazing⁵³ with increasing Σ overcomes the weakening due to phase separation. This may be helpful in the development of adhesion science.

4. Conclusions

In this paper, primitive path analysis, which has successfully been used to elucidate the nature of entanglements in polymer melts, was shown to give new insight into the properties of polymer brushes. For a brush in a small molecule solvent, modeled here as a continuum, implicit solvent, the extent of the entanglement density $\rho_e^{bb}(z)$ extends to larger heights as the coverage Σ increases, as expected. As the solvent quality decreases and the brush collapses, the number of brush–brush entanglements increases. A simple scaling argument for the total number of brush–brush entanglements gives results that are in very good agreement with the simulations.

As the molecular weight of the solvent increases, there is an entropic repulsion between the brush and the melt, and the melt chains are excluded from the brush. Here we studied the limiting case of a brush in contact with a highly entangled melt. As expected, both the peak in monomer density of the brush and in $\rho_e^{bb}(z)$ increase rapidly with increasing coverage. Over the range of coverages that we could study, the total number of brush–brush and brush–melt entanglements increased with increasing coverage. This is consistent with studies of the work of adhesion by Sides et al.,⁵³ who found that for the same coverages that the work of adhesion increased with increasing coverage. For larger coverages, it is expected that both the total number of entanglements and the work of adhesion would reach a peak and decrease for large coverages. However, as discussed by Sides et al., it is presently not possible to equilibrate systems for higher coverages than those studied here.

We also determined the melt–melt entanglement density both near the polymer brush and near a bare wall. Near a bare wall and near a wall containing a low polymer brush coverage, $\rho_e^{mm}(z)$ as shown in Figures 6 and 8 was 0 out to a distance of approximately 10σ and then reached a peak of about twice its value in the melt at a distance of approximately 20σ . For higher brush coverage, the melt chains were screened from the wall by the brush and $\rho_e^{mm}(z)$ increased monotonically away from the wall. The large gap in $\rho_e^{mm}(z)$ could partially be related to the primitive path analysis methodology, which fixes the chain ends and then pulls the chains taut.

Acknowledgment. Martin Kröger and Kurt Kremer provided useful discussions. The simulations in this paper were carried out using the LAMMPS molecular dynamics software (<http://lammmps.sandia.gov>). Figure 7 was produced using VMD.⁶⁹ This work is supported by the National Science Foundation under Grant No. DMR-0454947. Sandia is a multiprogram laboratory operated by Sandia Corp., a Lockheed Martin Co., for the United States Department of Energy's National Nuclear Security Administration under contract DE-AC04-94AL85000.

References and Notes

- Napper, D. H. *Polymeric Stabilization of Colloid Dispersions*; Academic Press: New York, 1984.
- Currie, E. P. K.; Norde, W.; Stuart, M. A. C. *Adv. Colloid Interface Sci.* **2003**, *100–102*, 205–265.
- Wool, R. P. *Polymer Interfaces: Structure and Strength*; Hanser: Munich, 1995.
- Léger, L.; Raphaël, E.; Hervet, H. *Adv. Polym. Sci.* **1999**, *138*, 185–225.
- Alexander, S. *J. Phys. (Paris)* **1977**, *38*, 983–987.
- de Gennes, P.-G. *Macromolecules* **1980**, *13*, 1069–1075.
- Milner, S. T. *Science* **1991**, *251*, 905–914.
- Grest, G. S.; Murat, M. In *Monte Carlo and Molecular Dynamics Simulations in Polymer Science*; Binder, K., Ed.; Oxford University Press: New York, 1995; p 476.
- Szleifer, I.; Carignano, M. A. *Adv. Chem. Phys.* **1996**, *94*, 165–260.
- Zhao, B.; Brittain, W. J. *Prog. Polym. Sci.* **2000**, *25*, 677–710.
- Milner, S. T.; Witten, T. A.; Cates, M. E. *Macromolecules* **1988**, *21*, 2610–2619.
- Milner, S. T.; Witten, T. A.; Cates, M. E. *Europhys. Lett.* **1988**, *5*, 413–418.
- Zhulina, E. B.; Borisov, O. V.; Pryamitsyn, V. A. *J. Colloid Interface Sci.* **1990**, *137*, 495–511.
- Murat, M.; Grest, G. S. *Macromolecules* **1989**, *22*, 4054–4059.
- Cosgrove, T.; Heath, T.; van Lent, B.; Leermakers, F.; Scheutgens, J. *Macromolecules* **1987**, *20*, 1692–1696.
- Chakrabarti, A.; Toral, R. *Macromolecules* **1990**, *23*, 2016–2021.
- Dickman, R.; Hong, D. C. *J. Chem. Phys.* **1991**, *95*, 4650–4665.
- Lai, P.-Y.; Binder, K. *J. Chem. Phys.* **1991**, *95*, 9288–9299.
- Lai, P.-Y.; Binder, K. *J. Chem. Phys.* **1992**, *97*, 586–595.
- Chakrabarti, A.; Nelson, P.; Toral, R. *Phys. Rev. A* **1992**, *46*, 4930–4934.
- Taunton, H. J.; Toprakcioglu, C.; Fetters, L. J.; Klein, J. *Nature* **1988**, *332*, 712–714.
- Taunton, H. J.; Toprakcioglu, C.; Fetters, L. J.; Klein, J. *Macromolecules* **1990**, *23*, 571–580.
- Patel, S. S.; Tirrell, M. *Annu. Rev. Phys. Chem.* **1989**, *40*, 597–635.
- Auroy, P.; Auvray, L.; Léger, L. *Phys. Rev. Lett.* **1991**, *66*, 719–722.
- Auroy, P.; Auvray, L.; Léger, L. *Macromolecules* **1991**, *24*, 2523–2528.
- Cosgrove, T. *J. Chem. Soc. Faraday Trans.* **1990**, *86*, 1323–1332.
- Cosgrove, T.; Heath, T. G.; Phipps, J. S.; Richardson, R. M. *Macromolecules* **1991**, *24*, 94.
- Field, J. B.; Toprakcioglu, C.; Ball, R. C.; Stanley, H. B.; Dai, L.; Barford, W.; Penfold, J.; Smith, G.; Hamilton, W. *Macromolecules* **1992**, *25*, 434–439.
- Raphaël, E.; Pincus, P.; Frederickson, G. H. *Macromolecules* **1993**, *26*, 1996–2006.
- Aubouy, M.; Raphaël, E. *J. Phys. II Fr.* **1993**, *3*, 443–448.
- Jones, R. A. L.; Norton, L. J.; Shull, K. R.; Kramer, E. J.; Felcher, G. P.; Karim, A.; Fetters, L. J. *Macromolecules* **1992**, *25*, 2359–2368.
- Nicolai, T.; Clarke, C. J.; Jones, R. A. L.; Penfold, J. *Colloids Surf. A* **1994**, *86*, 155–163.
- Clarke, C. J.; Jones, R. A. L.; Edwards, J. L.; Shull, K. R.; Penfold, J. *Macromolecules* **1995**, *28*, 2042–2049.
- Liu, Y.; Schwarz, S. A.; Zhao, W.; Quinn, J.; Sokolov, J.; Rafailovich, M.; Iyengar, W.; Kramer, E. J.; Dozier, W.; Fetters, L. J.; Dickman, R. *Europhys. Lett.* **1995**, *32*, 211–216.
- Zhao, X.; Zhao, W.; Rafailovich, M. H.; Sokolov, J.; Russell, T. P.; Kumar, S. K.; Schwarz, S. A.; Wilkens, B. J. *Europhys. Lett.* **1991**, *15*, 725–730.
- Budkowski, A.; Steiner, U.; Klein, J.; Fetters, L. J. *Europhys. Lett.* **1992**, *20*, 499–504.
- Budkowski, A.; Steiner, U.; Klein, J.; Fetters, L. J. *Macromolecules* **1993**, *26*, 2470–2478.
- Grest, G. S. *J. Chem. Phys.* **1996**, *105*, 5532–5541.
- Vilmin, T.; Tardivat, C.; Léger, L.; Brown, H.; Raphaël, E. *Europhys. Lett.* **2004**, *68*, 543–549.
- Doi, M.; Edwards, S. F. *The Theory of Polymer Dynamics*; Clarendon Press: Oxford, 1986.
- Everaers, R.; Sukumaran, S. K.; Grest, G. S.; Svaneborg, C.; Sivasubramanian, A.; Kremer, K. *Science* **2004**, *303*, 823–826.
- Sukumaran, S. K.; Grest, G. S.; Kremer, K.; Everaers, R. *J. Polym. Sci. Part B: Polym. Phys.* **2005**, *43*, 917–933.
- Fetters, L. J.; Lohse, D. J.; Richter, D.; Witten, T. A.; Zirkel, A. *Macromolecules* **1994**, *27*, 4639–4647.
- Kröger, M.; Hess, S. *Phys. Rev. Lett.* **2000**, *85*, 1128–1131.
- Fetters, L. J.; Lohse, D. J.; Milner, S. T.; Graessley, W. W. *Macromolecules* **1999**, *32*, 6847–6851.
- Fetters, L. J.; Lohse, D. J.; Graessley, W. W. *J. Polym. Sci. Part B: Polym. Phys.* **1999**, *37*, 1023–1033.
- Colby, R. H.; Fetters, L. J.; Funk, W. G.; Graessley, W. W. *Macromolecules* **1991**, *24*, 3873–3882.
- Inoue, T.; Yamashita, Y.; Osaki, K. *Macromolecules* **2002**, *35*, 9169–9175.
- Kröger, M.; Voigt, H. *Macromol. Theory Simul.* **1994**, *3*, 639–647.
- Ben-Naim, E.; Grest, G. S.; Witten, T. A.; Baljon, A. R. C. *Phys. Rev. E* **1996**, *53*, 1816–1822.
- Kremer, K.; Grest, G. S. *J. Chem. Phys.* **1990**, *92*, 5057–5086.
- Pütz, M.; Kremer, K.; Grest, G. S. *Europhys. Lett.* **2000**, *49*, 735–741.
- Sides, S. W.; Grest, G. S.; Stevens, M. J.; Plimpton, S. J. *J. Polym. Sci. Part B: Polym. Phys.* **2004**, *42*, 199–208.
- Graessley, W. W.; Hayward, R. C.; Grest, G. S. *Macromolecules* **1999**, *32*, 3510–3517.
- Karayiannis, N. C.; Mavrantzas, V. G.; Theodorou, D. N. *Phys. Rev. Lett.* **2002**, *88*, 105503.
- Auhl, R.; Everaers, R.; Grest, G. S.; Kremer, K.; Plimpton, S. J. *J. Chem. Phys.* **2003**, *119*, 12718–12728.

- (57) Frenkel, D.; Smit, B. *Understanding Molecular Simulations*, 2nd ed.; Academic Press: San Diego, CA, 2002.
- (58) Schneider, T.; Stoll, E. *Phys. Rev. B* **1978**, *17*, 1302–1322.
- (59) Zhou, Q.; Larson, R. G. *Macromolecules* **2005**, *38*, 5761–5765.
- (60) Tzoumanekas, C.; Theodorou, D. N. *Macromolecules* **2006**, *39*, 4592–4604.
- (61) Kröger, M. *Comput. Phys. Commun.* **2005**, *168*, 209–232.
- (62) Shanbhag, S.; Kröger, M. *Macromolecules* **2007**, *40*, 2897–2903.
- (63) Vladkov, M.; Barrat, J. L. *Macromolecules* **2007**, *40*, 3797–3804.
- (64) Meyer, H.; Kreer, T.; Cavallo, A.; Wittmer, J. P.; Baschnagel, J. *Eur. Phys. J. Spec. Top.* **2007**, *141*, 167–172.
- (65) Si, L.; Massa, M. V.; Dalnoki-Veress, K.; Brown, H. R.; Jones, R. A. L. *Phys. Rev. Lett.* **2005**, *94*, 127801.
- (66) Brown, H. R.; Russell, T. P. *Macromolecules* **1996**, *29*, 798–800.
- (67) Silberberg, A. *J. Colloid Interface Sci.* **1982**, *90*, 86–91.
- (68) Silberberg, A. *J. Colloid Interface Sci.* **1988**, *125*, 14–22.
- (69) Humphrey, W.; Dalke, A.; Schulten, K. *J. Mol. Graph.* **1996**, *14*, 33–38.

MA070943H